Progressive Investigation and Void Detection of Post-Tensioned Slab Bridge Tendons

Cameron Ward*, E.I.T., (presenting)
Mike Lau*, Ph.D., P.Eng., Partner
Ruth Eden**, M.Sc., P.Eng., Director
John Logan**, P.Eng., Consultant Services Engineer

* Dillon Consulting Limited
** Engineering and Operations Division, Water Control and Structures,
Manitoba Infrastructure and Transportation

Paper prepared for presentation
at the Bridge Session

of the 2012 Conference of the
Transportation Association of Canada
Fredericton, New Brunswick

Abstract

Twin bridge structures provide a grade separated crossing for Manitoba Provincial Trunk Highway (PTH) 8 over PTH 101. The superstructure consists of a continuous 5-span cast-in-place post-tensioned concrete slab. Constructed in 1973, the structures required a detailed condition assessment, strength evaluation, and preliminary design for rehabilitation. Due to the critical importance of the post-tensioning tendons to contribute to the load carrying capacity of the structure, it was determined that a progressive investigation and void detection assessment of the tendons was necessary.

Void detection testing of in-situ post-tensioning tendons was performed using the MALA Geoscience Imaging Radar Array (MIRA). Readings were obtained in the negative moment region where the tendons are nearest to the deck surface. Readings were obtained along one metre strips on both sides of all supporting structures. MIRA readings were verified by strip-removal of deck concrete and examination of tendons in four locations. The tendons were opened and examined for the presence of voids, grout was sampled for chloride content, and the strands were inspected for signs of distress.

The detailed condition assessment was carried out in accordance with the Ministry of Transportation Ontario (MTO) Structure Rehabilitation Manual and consisted of visual inspection, concrete cover measurements, delamination survey, corrosion potential readings, and a coring program to determine concrete compressive strength, chloride content, air-void content, and to perform petrographic analysis.

Strength evaluation (load rating) of the twin structures was carried out in accordance with the AASHTO Manual for Bridge Evaluation (2nd Edition, 2011) under the Strength I limit state. Trucks evaluated were the HS 25 lane, HS 30 lane, HSS 25 truck, HL-93 design truck, and TAC legal loads (39.5, 56.5, and 62.5 tonne configurations). The structure was designed for the HS 20-44 live load.

The progressive investigation and void detection assessment of the tendons was an important part of the condition assessment and vital for the accurate strength evaluation of the twin structures.

1.0 INTRODUCTION

1.1 Background

Similar to most jurisdictions, Manitoba Infrastructure and Transportation (MIT) has adopted an asset management hierarchy consisting of preservation, rehabilitation, and finally replacement. Because many structures currently in service are reaching the end of their design lives, rehabilitation is the primary course of action to extend the life of a structure an additional 30 to 40 years where possible. The twin overpass structures on Provincial Trunk Highway (PTH) 8 over PTH 101 are such structures requiring major rehabilitation.

This paper describes the detailed condition survey and tendon investigation program implemented to determine the condition of the bridge structures. This information was used to evaluate the structural capacity of the bridge and to develop a number of preliminary design alternatives for the rehabilitation of the structures.

1.2 Description of the Facility

The twin overpass structures on PTH 8 (north-south) over PTH 101 (east-west) provide an important grade separation for two busy highways in the capital region, as shown in Figure 1. The grade separation takes the form of a cloverleaf, with an additional collector-distributor (CD) lane available to westbound PTH 101 traffic for access to northbound and southbound PTH 8. The annual average daily traffic (AADT) on PTH 8 and PTH 101 is 17 630 and 21 300 respectively (2010 data) [1]. The annual average daily truck traffic (AADTT) is 800 and 2 500 respectively (2008 data) [2]. The bridge structures are, for all intents and purposes, symmetrically identical, thus moving forward, the twin structures will simply be described in the singular.

Figure 1: Aerial photo showing the grade separated interchange.

There is no posted weight restriction on the bridge, thus the highest live load is the 62.5 tonne TAC legal load configuration. Constructed in 1973, the bridge was designed in accordance with AASHTO 10th Edition 1969 and Interim Specifications and to a live load of H20-S16-44. The structure is a post-tensioned slab bridge, situated at a skew of 7˚57'20". Span lengths (south to north) measure 20 569, 20 117, 15 240, 17 983, and 18 436 mm. The superstructure consists of a continuous solid concrete post-tensioned slab 559 mm (22 in) thick, measuring 14 630 mm (48 ft) wide. Expansion joints are present at both abutments. 1 219 mm (4 ft) and 914 mm (3 ft) wide voided curbs are present on the left and right side of the roadway respectively. The remaining roadway is divided into three lanes (two through and one merge/egress) and shy and shoulder room. The slab is directly supported by four column bents (piers) each consisting of four columns. The two center column bents are supported on bearings fixed to translation in the longitudinal direction, whereas the remainder of the column bents and abutments feature expansion bearings. The columns themselves are 762 mm (30 in) in diameter and spaced at 3 956 mm (12 ft 11¾ in). A bridge cross-section is presented in Figure 2.

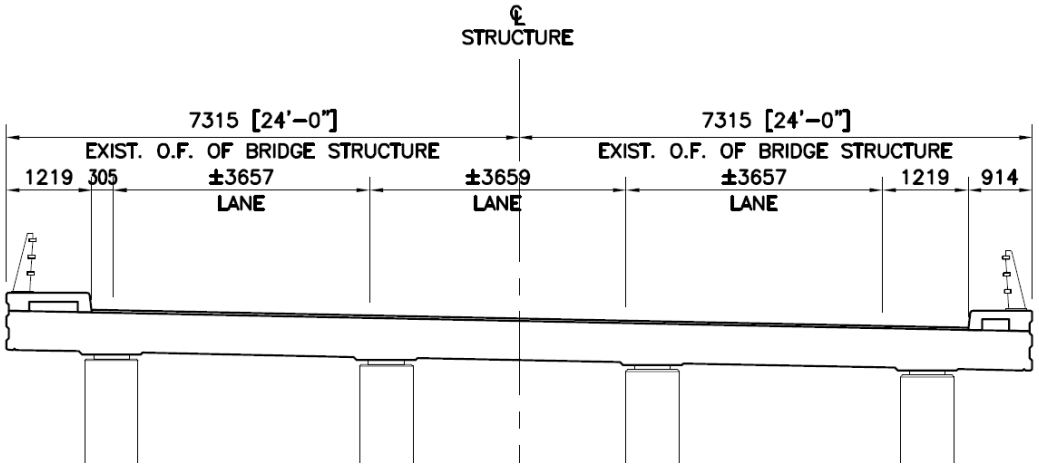

Figure 2: Typical cross-section of the bridge structure

The post-tensioning system is comprised of 51 ducts spaced at 286 mm (11 ¼ in). The depth from the top of the slab to the centerline of the ducts is identical for all ducts and varies based on the presence and magnitude of the positive and negative longitudinal bending moments experienced by the slab, from a maximum of 432 mm (17 in) at mid-span locations to a minimum of 140 mm (5½ in) over piers. Each duct contains twelve 0.5 in diameter Freyssinet multistrands with a minimum of 1 860 MPa (270 ksi) ultimate tensile stress. The ducts are three inch diameter galvanized semi-rigid type with fully grouted multistrands. Record drawings indicate grout vents were provided at low and high points in the tendon profile. The specified strength of the concrete slab was 38 MPa (5 000 psi).

2.0 DETAILED CONDITION SURVEY

A detailed condition survey (DCS) was performed on the twin structures in accordance with the Ontario Ministry of Transportation (MTO) Structural Rehabilitation Manual [3]. In addition to

detailed visual inspection, a number of parameters were measured including concrete cover, corrosion potential, chloride content, air-void parameters, concrete compressive strength, and finally petrographic examination of concrete. To measure chloride content, air-void parameters, compressive strength and to perform petrographic examination, a number of concrete cores were obtained from various structural elements. The coring program undertaken is described in Table 1.

Table 1: Detailed condition survey coring program

Structural Element	Number of Concrete Cores per Structure			
	Chloride Content	Air-Void Parameters	Compressive Strength	Petrographic Examination
Deck	10	2	5	2
Curb	2	0	0	0
Abutments	2	0	2	0
Piers	8	0	4	0
Total	22	2	11	2

Presentation of the results of the DCS is divided into the main points for the deck surface, deck soffit, concrete curbs, joints, rails and posts, abutments and wingwalls, and finally piers. Numeric values are presented for northbound (NB) and southbound (SB) structures. It should be noted that the typically accepted threshold value for the water soluble chloride content in concrete to initiate corrosion is 0.025% by mass, and that if corrosion potentials over an area are more negative than -0.350V, it is generally considered that there is a greater than 90% probability that reinforcing steel corrosion is occurring in that area at the time of measurement.

2.1 Deck Surface

- Cover ranged from 0 mm to 97 mm with an average of 32 mm (NB) and 26 mm (SB).
- Average compressive strength was 38.5 MPa (NB) and 43.8 MPa (SB).
- Seven of the ten cores have chloride content at the rebar level more than the threshold value of 0.025% (NB). Eight of the nine cores have chloride content at the rebar level more than the threshold value of 0.025% (SB).
- The hardened air void parameters meet the current CSA standards (NB and SB structures).
- Petrographic examination revealed that the Damaged Rating Index (DRI) is very low for all deck slab cores, indicating good condition of the concrete.
- Corrosion potential ranged from -0.001V to -0.565V with an average of -0.139V (NB) and -0.180 (SB). The statistical corrosion potentials for the entire deck are shown in Table 2.

Table 2: Corrosion potential summary for NB and SB structures

Northbound Structure		Southbound Structure	
Percent of Deck Area	**Corrosion Potential**	**Percent of Deck Area**	**Corrosion Potential**
75% (869 m^2)	< -0.2V	66% (759.5 m^2)	< -0.2V
18% (205 m^2)	-0.200V and -0.350V	24% (279.8 m^2)	-0.200V and -0.350V
7% (78 m^2)	> -0.350V	10% (115 m^2)	> -0.350V

2.2 Deck Soffit

- Visual inspection shows only that the areas of concern are exterior and end soffits (as well as fascias) within 2.0 m from the edges.
- More than 20% (NB) and 18% (SB) of the area has corrosion potential more negative than -0.350V, mostly occurring at the fascias.
- Average concrete cover is 26 mm (NB) and 27 mm (SB) for soffit.
- At the exterior fascias the average cover ranged from 2 mm to 82 mm with an average of 49 mm (NB) and 52 mm (SB), lower than the specified 62 mm.
- Chloride profile tests on one core taken from the fascia indicated high chloride contents up to a depth of 80 mm.

2.3 Concrete Curbs and Newel Posts

- Visual inspection observed various degrees of delaminations, spalling, and sporadic areas of repair patches.
- Average concrete cover readings average 53 mm (NB) and 62 mm (SB). Cover is greater than the specified 50 mm.
- Chloride contents measured from one core per curb indicate values in excess of the threshold value.
- A total of 230 m^2 or 92.5% (NB) and 192 m^2 or 77.3% (SB) of the area has corrosion potential more negative than -0.350V.

2.4 Joints

- Debris was noted within the expansion joints. Cracks were noted in the joint seals. Water was observed leaking through the joints. Delamination on the soffit was noted at the abutments.

2.5 Rails and Posts

- The steel hand rails appeared to be in good condition with the exception of some localized corrosion. Vehicular impact damage was noted at several locations.

2.6 Abutments and Wingwalls

- Visual inspection noted spalls at the ends/corners. Medium cracks were noted at several locations. Water as well as debris was observed on the bearing seats, indicating joint leakage. Light corrosion is common on all bearing plates.
- Average concrete cover for abutments was 73 mm (NB) and 70 mm (SB). Specified cover was 75 mm.
- Average concrete cover for the wingwalls was 64 mm (NB) and 56 mm (SB). Specified cover was 50 mm.
- The average compressive strength was 48.4 MPa (NB) and 54.7 MPa (SB).
- The chloride contents at the average reinforcing steel depth ranged from 0.114% to 0.316% (NB) and from 0.206% to 0.273% (SB).
- The NB abutments had a total of 55.8 m^2 (95%) of the surface with corrosion potential more negative than -0.350V. The SB abutments had a total of 67.8 m^2 (98%) of the surface with corrosion potential more negative than -0.350V.
- NB wingwalls had a total of 4.6 m^2 (58%) of the surface with corrosion potential more negative than -0.350V. SB wingwalls had a total of 5.6 m^2 (69.2%) of the surface with corrosion potential more negative than -0.350V.

2.7 Piers

- Visual inspection noted a layer of cementitious coating on all piers, as well as minor spalling caused by popouts of coarse aggregates.
- The average concrete cover was 55 mm (NB and SB). Specified cover was 50 mm.
- The average compressive strength was 62.3 MPa (NB) and 67.8 MPa (SB).
- The chloride content at the average reinforcing depth of 55 mm is estimated to range from 0.009% to 0.302%. For NB and SB structures, two of the eight cores had chloride content greater than the threshold at the rebar level.
- Average corrosion potential of the piers was -0.112V (NB) and -0.091V (SB).

3.0 TENDON INVESTIGATION

To gain confidence in the condition of the post-tensioning system, a progressive tendon investigation was carried out. Typical deficiencies encountered during investigation of PT systems include discovery of either incomplete grouting of the PT ducts or corrosion of the strands themselves. Both deficiencies may act to reduce the PT system's structural capacity.

3.1 Strand Corrosion Investigation

Stress corrosion cracking (SCC) is the cracking induced from the combined influence of tensile stress and a corrosive environment. SCC is a risk in almost all pre-stressed and post-tensioned concrete bridge elements; however, this risk is greater for pre-stressed or post-tensioned deck slabs (compared to girders for example) as the de-icing compounds are applied directly to the slab, whereas in the case of girders, the strands are protected from direct chemical attack by a concrete deck. Thus, to closely examine the strands for evidence of SCC and corrosion in general, it was necessary to expose the strands.

Strands were exposed in four locations (two per structure). One of the exposures for each structure was carried out in an area of high corrosion potential, as this was thought to be the most likely location of corrosion in the strands. The duct was opened up and grout removed to expose the strands. A sample of the grout was obtained for chloride content testing. The average chloride content in the grout was measured to be 0.008%, with the highest single chloride content being 0.016%. The exposed strands were visually inspected for signs of corrosion. Figure 3 illustrates the typical condition of the PT grout and strands. No corrosion of the strands was observed.

(a) (b)

Figure 3: Typical condition of a) grout and b) exposed strands after grout removal

Strands were also exposed in locations to verify the results of the void detection testing, as described in the next section.

Once the necessary inspections were completed, the exposed strands were covered in a thick coating of two-part epoxy, which was allowed to cure. Grout was then used to replace excavated concrete.

3.2 Void Detection Testing

The problem of aging infrastructure has promoted development in the area of non-destructive testing (NDT). Non-destructive tests may be used to monitor structures and reveal safety hazards. Furthermore, they may be used to determine the properties of various civil structures in-situ in order to most effectively rehabilitate structures. There are many NDT capable of characterizing materials and defects, including but not limited to simple visual inspection, acoustic sounding, liquid penetrant methods, impulse response, impact-echo, and infrared thermography [4]. One method that has a proven track record in flaw detection is reflection-based ultrasonic methods, also known as the pulse-echo method. The method has been used extensively in the quality control of welds, as well as routine use for inspections in the aerospace industry. Its use in detecting internal flaws in concrete, including void detection in post-tensioned systems, has been gaining popularity [5-7].

In the case of the presence of voids, a lack of grout can open the strands up to corrosion as the grout acts as a protective barrier to corrosion-inducing conditions. Imperfectly grouted tendons can allow water to build up in the voids, promoting corrosion of the strands. Additionally, a lack of grout can cause the PT system to inadequately transfer PT forces from the steel to the concrete, resulting in the system not functioning as intended. To verify that the PT ducts were fully grouted, an ultrasonic tomographer was used to non-destructively investigate the tendons.

The method works due to the fact that concrete and void (i.e. air) have a large impedance mismatch, resulting in a high amplitude ultrasonic wave reflecting off the concrete-void interface. By contrast, the impedance mismatch between concrete and grout is small, thus the reflected wave has low amplitude. When transducers are arranged in an array, transmitted and reflected data is transformed into a visual representation of the element under investigation using post-processing algorithms.

The apparatus used to perform non-destructive testing for the current study was the MALA Geoscience Imaging Radar Array (MIRA). The MIRA makes use of ultrasonic shear waves to detect flaws (discontinuities) in concrete. The system is capable of generating 3D tomographic images of the area under investigation. Shear waves are used rather than longitudinal (compression) waves because research has shown that shear waves reduce the amount of backscattering and signal attenuation in the direction parallel to the propagating wave [8, 9].

The device used to obtain the data consists of 40 spring-loaded dry point contact (DPC) transducers arranged in a 4 x 10 grid. The dry point contact technology eliminates the need for the regular re-application of a coupling agent. Due to the large number of shots required, the elimination of this step significantly reduces the time needed for data acquisition. The MIRA apparatus is shown in Figure 4.

Figure 4: View of the shear wave ultrasonic tomography MIRA system [9]

Each "shot" obtains a virtual slice of the element being investigated. A shear wave is emitted by the transducer array and received after reflecting off internal surfaces. The data is wirelessly transmitted to an on-site computer and processed in a matter of seconds. The image reconstruction software employs an algorithm that uses the 3D synthetic aperture focusing technique (SAFT), improving the resolution of the ultrasonic image [9].

Tendons were tested over a 1.0 m long strip on either side of each pier. Readings were obtained near piers (i.e. in negative moment regions) because those are the locations where the strands are nearest the slab surface, and therefore most likely to experience corrosion. Readings were not obtained directly over the centerline of the piers due to the large number of reinforcing bars present at this location, acting as a hidden transfer beam within the slab, which makes locating the PT duct and interpretation of the void detection data problematic.

3.2.1 Procedure

Work began by stripping the asphalt concrete wearing surface and waterproofing membrane off the PT concrete slab. Removal of the asphalt overlay is required before proceeding with acquiring MIRA readings, as the impedance mismatch between the asphalt and concrete does not allow for transmission of the shear wave into the concrete slab. Stripping was performed with a hydraulic hammer mounted to a small excavator.

Asphalt was removed for an approximately 4 m long strip over each pier for the full width of the bridge between curb faces. Following stripping of the asphalt, the concrete slab surface was thoroughly cleaned of debris. Any remaining waterproofing membrane or bituminous substance adhering to the concrete surface was removed by vibratory chisel, fitted with a scraper.

First, the limits of the void detection scans were marked out (1.0 m wide strip on either side of the pier). Ground penetrating radar (GPR) was used to determine the location of the centerline of each PT tendon on each side of the exposed slab. The centerline of the tendon was marked with a chalkline over the limits for void detection scans. Once the tendons were located and marked, the scan "shot" locations were marked on the tendon ceneterlines. These were spaced at approximately 50 mm. Once the layout of "shots" was completed, the MIRA system was used to gather the data.

Data was acquired by a single worker, each shot taking approximately 3-5 seconds to obtain. Thus, a tomograph for a 1.0 m long section of tendon took about one minute to acquire. Once the data for a particular section of the concrete slab was obtained, the asphalt wearing surface was replaced.

3.2.2 Results and Verification

The results of the void detection testing are best presented as various degrees of the relative probability of voids including high, medium, and low. Figures 5, 6, and 7 present typical tomography for each case. Each tomograph shows a plan, section, and elevation view of the three dimensional image generated.

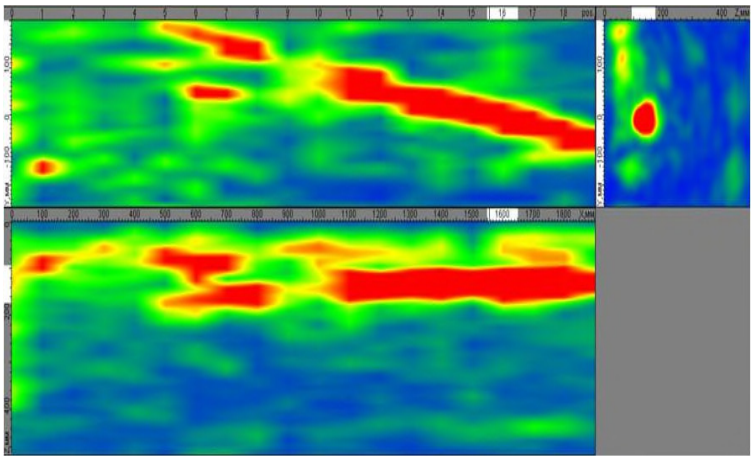

Figure 5: Tomograph representative of a high probability of voids

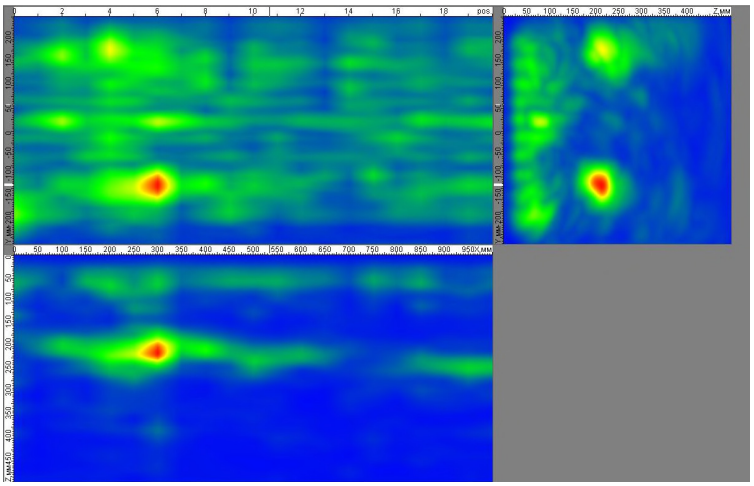

Figure 6: Tomograph representative of a medium probability of voids

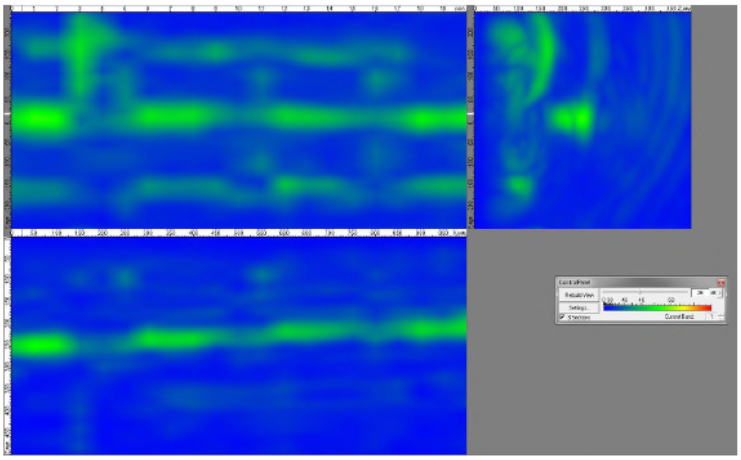

Figure 7: Tomograph representative of a low probability of voids

Once all tendon data was collected, it was analyzed and reviewed. The number of instances of each probability was determined, as shown in Table 3 and 4, for the NB and SB structures respectively.

Table 3: Probability of voids for NB structure

Probability of Voids	Number of Readings				
	SU2	SU3	SU4	SU5	Total
Unreadable	1	3	0	12	16
High	0	0	0	0	0
Medium	0	0	0	0	0
Low	85	79	84	74	322
Total	86	82	84	86	338

Table 4: Probability of voids for SB structure

Probability of Voids	Number of Readings				
	SU2	SU3	SU4	SU5	Total
Unreadable	0	0	0	0	0
High	0	0	0	0	0
Medium	0	0	0	2	2
Low	84	84	88	85	341
Total	84	84	88	87	343

The cause of "unreadable" data points was localized spalling of the concrete surface. In some areas, portions of the surface of the concrete slab had spalled off leaving a rough depression. Non-destructive testing data could not be obtained due to imperfect contact between the concrete surface and the transducer array at these locations.

The findings of the void detection testing were verified by performing two duct exposures on each structure. As mentioned, one of the exposures was performed in an area of high corrosion potential to examine the strands for corrosion. The second location was performed in an area of high probability of voids relative to other readings. Once the void detection testing was complete for a given section of the concrete slab, the results were reviewed in the field, and the location of the duct exposure determined. Unfortunately, due to traffic staging requirements of the project, the location exposed was not necessarily always in the area of overall highest probability of voids. Nonetheless, a location was chosen based on field analysis of the data available at that time. Similar to the tendon exposures described above for inspection of the strands for corrosion, the ducts were exposed and opened to expose the grout. The exposed area was inspected for the presence of voids. Despite some variability observed in the relative probability of voids in the ducts, tendon exposures suggested that the ducts were in fact fully grouted. A potential cause of apparent voids in the duct may be caused by low amplitude reflections. These reflections may be due to a) shrinkage of the concrete or grout, causing a very small separation between the concrete/grout and the duct material, b) corrugations in the duct (approximately

one mm wide) may not have been fully filled with grout, presenting a discontinuous system of very small voids in the duct, or c) small air bubbles present in the grout observed along the top of the exposed grout.

Once the grout was inspected, a portion of it was removed to expose the strands, which were inspected for corrosion. Again, a sample of grout was retrieved for chloride content testing.

4.0 STRENGTH EVALUATION AND DEVELOPMENT OF REHABILITATION ALTERNATIVES

The condition factor is a factor which provides a reduction to account for the increased uncertainty in the resistance of deteriorated members and the likely increased future deterioration of the members. Based on the findings of the detailed condition survey and tendon investigation, the post-tensioned slab's capacity was determined assuming no reduction in structural performance, thus the condition factor was taken as $\varphi_c = 1.0$ [10].

For most major rehabilitation projects, Manitoba Infrastructure and Transportation specifies a design live load of HSS 25, whereas for new construction, HSS 30 is specified. Analysis of the slab was performed with the following live loads:

- Design Loads: HS 25 lane, HS 30 lane, HSS 25 truck, HL-93 design truck, and;
- TAC Legal Loads: 39.5, 56.5, and 62.5 tonne configurations.

The Strength I load case was investigated in accordance with the AASHTO Manual for Bridge Evaluation [10]. It was determined that the governing live load for flexure and shear in the slab was the HSS 25 (truck) configuration. The critical rating factors in the slab in flexure and shear under this live load were determined to be 1.56 and 2.79 respectively. Although the findings of the strength evaluation suggest an increase in the allowable design live load is permissible in the ultimate limit states, it was recommended that a detailed structural assessment be performed in the service limit states to investigate if an increased design live load would result in cracking of the concrete. Cracking of the concrete slab is viewed as undesirable (especially in negative moment regions) because it will increase the rate of ingress of corrosion inducing substances to the level of post-tensioning strands.

A number of rehabilitation options were considered for the concrete slab, including a "do nothing" option, concrete patch repairs, variable-partial depth rehabilitation of the slab (deeper in areas of poor concrete), and finally complete partial depth rehabilitation of the concrete slab. Taking into consideration the findings of the detailed condition assessment, importance of the post-tensioning system to the strength and safety of the structure, and life-cycle analysis of the rehabilitation options, the preferred option was determined to be complete partial depth rehabilitation of the concrete slab to a depth of approximately 100 mm.

5.0 CONCLUSIONS AND RECOMMENDATIONS

To develop an effective rehabilitation program for the twin overpass structures at PTH 8 over PTH 101, a detailed condition survey and tendon investigation was carried out. The tendon investigation included ultrasonic void detection testing in negative moment regions. Tendons were exposed in selected areas to verify the results of the void detection testing as well to inspect for electrochemical corrosion of the strands. A strength evaluation was carried out in accordance with the AASHTO Manual for Bridge Evaluation, and rehabilitation options were developed at a preliminary design stage.

Non-destructive void detection testing is a low cost and non-invasive method to obtain information on PT systems and should be used to complement traditional detailed condition surveys.

PT strands are a critical structural component of any PT element, and therefore the condition of the system should be thoroughly investigated during bridge condition surveys.

Corrosion investigation of the strands should be carried out in areas of negative bending moment (i.e. over piers) because these locations have strands nearest to the surface (least concrete cover), coupled with the fact that negative moment cracking in the concrete may promote downward ingress of corrosion-inducing substances.

Void detection investigation of the ducts should also be carried out in areas of negative bending moment because the PT profile is maximum in these regions, resulting in higher probability of imperfect grouting of the ducts in these locations.

The ultrasonic method presented can be used effectively on flat and macroscopically smooth concrete surfaces. In some areas, portions of the surface of the concrete slab had spalled off leaving a rough depression. Non-destructive testing data could not be obtained due to imperfect contact between the concrete surface and the transducer array in these locations.

The results of the non-destructive void detection investigation of the post-tensioned slabs agreed with the findings of strand exposure in four locations.

Taking into consideration the findings of the detailed condition assessment, importance of the post-tensioning system to the strength and safety of the structure, and life-cycle analysis of the rehabilitation options, the preferred option was determined to be complete partial depth rehabilitation of the concrete slab to a depth of approximately 100 mm.

6.0 REFERENCES

[1] University of Manitoba Traffic Information Group. “Annual average daily traffic on provincial trunk highways and provincial roads.” Internet: http://umtig.eng.umanitoba.ca/tis_web_2010/flowmaps/flowmap2010.pdf, April 2011 [accessed March 20, 2012].

[2] University of Manitoba Traffic Information Group. “Annual average daily truck traffic on provincial trunk highways and provincial roads.” Internet: http://umtig.eng.umanitoba.ca/tis_web_2010/flowmaps/TruckFlowMap2008.pdf, March 2010, [accessed March 20, 2012].

[3] Ministry of Transportation Ontario. *Structure Rehabilitation Manual*. Revision #10, April 2007.

[4] C.C. Ferraro. “Advanced non-destructive monitoring and evaluation of damage in concrete materials”. Masters thesis, University of Florida, United States, 2003.

[5] O. Abraham and P. Cote. “Impact-echo thickness frequency profiles for detection of voids in tendon ducts.” *ACI Structural Journal,* 99(3), pp. 239-247, May 2002.

[6] Shivprakash R. Iyer, Sunil K. Sinha, and Andrea J. Schokker. “Ultrasonic C-Scan imaging of post-tensioned concrete bridge structures for detection of corrosion and voids.” *Computer-Aided Civil and Infrastructure Engineering,* 20(2), pp. 79–94, March 2005.

[7] N. Alver, M. Tokai, and Y. Nakai. “Identification of imperfectly-grouted tendon duct in concrete by SIBIE procedure.” in *NDT for Safety*, Prague, November 7-9, 2007, pp.9-14.

[8] A.A. Samokrutov, V.N.Kozlov, and V.G.Shevaldykin. “Ultrasonic examination of concrete structures”.

[9] Aldo O. De La Haza, Claus Germann Petersen, and Andrey Samokrutov. “Three dimensional imagaing of concrete structures using ultrasonic shear waves.” Internet: http://acsys.ru/eng/article/files/Imaging_of_concrete_structures.pdf, date unknown, [accessed November 5, 2011].

[10] American Association of State Highway and Transportation Officials. *Manual for Bridge Evaluation*, Second Edition (2010) plus 2011 interim revisions.

Acknowledgements

Manitoba Infrastructure and Transportation (bridge owner).

Vector Construction Inc. for their participation in the void detection testing.

Stantec Inc. for their participation in the detailed condition survey.